Journal of Materials Chemistry A

Accepted Manuscript

ROYAL SOCIETY OF CHEMISTRY

www.rsc.org/materialsA

Journal Name

ARTICLE

Trimodal hierarchical carbide-derived carbon monoliths from steam- and CO_2-activated wood templates for high rate lithium sulfur batteries

Received 00th January 20xx,
Accepted 00th January 20xx

DOI: 10.1039/x0xx00000x

www.rsc.org/

Marion Adam[a], Patrick Strubel[b], Lars Borchardt[a], Holger Althues[b], Susanne Dörfler[b], and Stefan Kaskel [a,b,]†

Hierarchically structured biomorphic carbide-derived carbon (CDC) materials are obtained by applying a combined activation- and CDC approach on an abundantly available, renewable and cheap raw material.. For the synthesis of these materials we mimic nature by using wood structures as templates which are already optimized for mass transport during their long-term evolutional process. The impregnation of the steam- or carbon dioxide- pre-activated wood templates with a polycarbosilane precursor and the subsequent halogen treatment yields a hierarchical material that exhibits longitudinal orientated macropores from the wood structure as well as well-defined and narrowly distributed micro- and mesopores derived from the activation and CDC approach. These materials offer specific surface areas up to 1750 m^2/g, micro-/mesopore volumes up to 1.0 cm^3/g and macropore volumes of 1.2 cm^3/g. This sophisticated hierarchical pore system ensures both efficient mass transfer and high specific surface area, ideal for mass transport limited applications, which we like to demonstrate exemplarily in the LiS battery application. Testing steam activated wood-CDCs as cathode material in Li-S batteries reveals excellent performance, especially a highly stable discharge capacity and sulfur utilization. Stable capacities of over 580 mAh/g_{sulfur} at current densities exceeding 20 mA/cm^2 (2 C) are possible using only very low amounts of electrolyte of 6.8 $\mu l/mg_{sulfur}$.

Introduction

Porous carbon materials have gained considerable attention in the last years due to their high chemical and thermal stability, tunable pore size distribution, and high specific surface areas (SSAs), which lead to a wide range of potential applications, such as catalysis[1,2], gas separation/adsorption[3,4], and electrochemical energy storage[5,6]. However, in many applications a high specific surface area combined with advanced mass transport kinetics is of great interest. Therefore, the focus in the last years is on the synthesis of hierarchically structured carbons, where meso- or macropores can be achieved via various template concepts[1,7-9]. These approaches tend to be complex, laborious, time-consuming and the template itself often has to be expensively synthesized. Under these considerations, natural templates[10-16] offer several advantages that are: their abundant availability, renewability and considerably low price. Moreover, bio-templates like wood already possess a hierarchical cell anatomy that is optimized for mass transport during a long-term evolutional process. This makes these materials particularly interesting for applications where enhanced mass transport kinetics are indispensible. However, beside a good transport pore system, high specific surface areas, usually provided by micropores are highly desired for various applications. Much research has been carried out on chemical and physical activation of wood or wood-derived materials resulting in a variety of porous activated wood materials with high porosity[17-21]. Nevertheless, a high specific surface area can only be achieved at high activation levels, which involves a large destruction of the cell walls and a broad pore size distribution[19-20].

The carbide-derived carbon (CDC) approach is a well-known possibility to obtain carbon materials with high SSA and a very narrow pore size distribution[6,8,22]. They are synthesized due to the selective removal of metal or semi-metal atoms from carbide precursors by hot halogen treatment. The porosity of CDCs can be controlled by the choice of the carbide precursor and the halogen treatment conditions[23]. Recently, we have shown that the combination of synthetic templates and the CDC approach allows to access hierarchical carbon materials with high SSA (up to 3000 m^2/g) and well-defined transport pore systems[1,7,24]. Hence, the use of biotemplates is the next step for synthesis of innovative materials. Combining the CDC approach and wood as template is of considerable interest because the longitudinal orientated macropore system promotes high availability.

In a first proof-of-principle[25] we have recently shown that hierarchical wood-derived CDC materials can be synthesized. However, only moderate surface areas have been obtained and

[a] Department of Inorganic Chemistry, Dresden University of Technology, Bergstraße 66, 01062 Dresden, Germany
[b] Fraunhofer Institute of Material and Beam Technology, Winterbergstraße 28, 01277 Dresden, Germany

† Corresponding author. Phone: +49-35146333632. E-mail address: stefan.kaskel@chemie.tu-dresden.de

Electronic Supplementary Information (ESI) available: [details of any supplementary information available should be included here]. See DOI: 10.1039/x0xx00000x

several infiltration steps or long infiltration times of the carbide precursor were necessary. Here we show how a pre-activation step with carbon dioxide or steam allows for both; higher surface areas and only a single impregnation step. We like to show, that this preparation concept enables the combination of the benefits of the individual techniques with the wood template to produce carbon materials with high specific surface areas up to 1750 m^2/g but also narrow nanopore size distribution. Hierarchical CDC materials with large transport pores can be synthesized, interesting as electrode material for Li-S batteries, due to maintaining the unique wood microstructure with longitudinal orientated wood cells/macropores during the whole preparation process.

Sulfur is a cheap and non-toxic element with a high theoretical capacity of 1672 mAh/g[26,27]. However, despite intensive research focus in the last 10 years still challenges need to be addressed such as low sulfur utilization, cycle stability, coulombic efficiency as well as rate performance[28]. Introduced by Nazar's group in 2009, a large number of novel approaches have been explored to bear down the main disadvantages of the Li-S batteries[29-32]. However, studies under practically relevant conditions, that are high sulfur loading, high electrode density, and low excess of electrolyte are rather scarce. This may play an important role at high C-Rates due to the strong influence on the electrochemical kinetics. Hierarchical porous carbon materials having both, *reaction*- and *transport* pores may be advantageous because transport pores allow the rapid ion transport (and thus faster charge–discharge rates), while micropores induce reduced polysulfide dissolution and provide high surface area for sufficient electrical contact between sulfur and carbon[33,34]. Hence, we will show that the activated wood-CDC material shows remarkable rate stability at high current densities exceeding 20 mA/cm^2, applied in the lithium sulphur battery.

Experimental

Material synthesis

Preparation of biotemplate. Birch wood (*Betula verrucosa*) was used as biotemplate for the synthesis of biomorphic CDC materials. The natural birch samples were cut in discs of approximately 1 g, 10 mm in diameter and 20 mm in height, cleaned from bark, and dried (80 °C, 24 h in air).

Steam activation. For steam activation, birch monoliths were placed in a horizontal quartz tube furnace and heated at a rate of 450 K/h from room temperature to 450 °C. At this temperature, the samples were treated with steam for 1.5 h. Steam was generated in the furnace by flushing with wet argon. Therefore, argon at a flowing rate of 80 ml/min was bubbled through deionized water in a heated flask. The water saturation of argon flow was adjusted with the water temperature of 25 °C, 50 °C, or 80 °C. After this treating step at 450 °C, the oven was heated to 900 °C in argon atmosphere and kept at this point for 5 h with steam.

CO_2 activation. Prior to carbon dioxide activation, the birch monoliths were pyrolyzed in argon flow at 800 °C for 3 h. Afterwards, the activation experiments were carried out at 850 °C, 900 °C, and 950 °C for 2 h with carbon dioxide, heating with 100 K/h to desired temperature and cooling were performed under argon atmosphere.

Synthesis of activated wood-CDCs. The activated wood monoliths were immersed with allylhydridopolycarbosilane (SMP-10, Starfire Systems) for 24 h at room temperature. The impregnated wood samples were dried over night (80 °C in air) and then pyrolyzed (800 °C, 3 h under an argon flow, 100 K/h heating rate) yielding *bio*C/SiC. Afterwards, a chlorine treatment was applied to remove silicon from SiC, yielding the activated wood-CDC. The samples were transferred in a horizontal quartz tube furnace and heated to 800 °C (450 K/h heating rate) with an argon flow of 150 mL/min. The gas flow was subsequently changed to a mixture of 80 mL/min chlorine and 70 mL/min argon while the temperature was maintained at the same level for 3 h. Finally, the chlorinated samples were treated with hydrogen for 1 h at 600 °C (80 mL/min) to remove residual chlorine species from the surface of the materials.

Nomenclature. The activated samples are specified with the activation method (CO_2 or H_2O) and the activation temperature in the case of carbon dioxide (850, 900 or 950) and the temperature of water in the case of steam activation (25, 50 or 80). The intermediate *bio*C/SiC is marked with –SiC and the resulting CDC materials with –CDC.

Material characterization

On Autosorb 1C (Quantachrome Instruments) nitrogen physisorption measurements were performed at 77 K. SSAs were calculated using the equation from Brunauer, Emmett and Teller (BET) in relative pressure range of 0.05 – 0.20 p/p_0. Using the Quenched Solid Density Functional Theory (QSDFT) method for carbon (slit-cylindrical pores, adsorption branch kernel) the presented pore size distributions were calculated. Micropore volumes were calculated with QSDFT from the cumulative pore volumes at a pore diameter of 2 nm and total mesopore volumes at 30 nm pore diameter. Prior to nitrogen physisorption experiments, all samples were activated at 150 °C for 24 h under vacuum. Mercury intrusion porosity was performed using a PASCAL440 (Thermo Fisher Scientific). Scanning electron microscopy (SEM) images and energy dispersive X-ray analysis (EDX) were acquired with a DSM-982 Gemini (Zeiss) at an acceleration voltage of 8 kV in the case of SEM and 20 kV in the case of EDX. Powder XRD was performed on an X'Pert diffractometer (PANalytical) in Bragg_Brentano geometry (Cu K_{alpha} radiation, λ = 0.15405 nm). Thermal analyses were performed under ambient pressure in air or inert atmosphere using a DTA-DSC Labsys TMA system (Setaram) with a heating rate of 5 K/min.

Electrochemical characterization

Composite preparation. The C/S composite was prepared by carefully mixing of the porous carbon material (reference material or H_2O50-CDC) and pristine sulfur (Sigma Aldrich, ≥ 99.5 %) in a porcelain mortar. According to the different pore volume, the weight ratio of carbon-to-sulfur was adjusted to 1 : 0.24 for reference and 1 : 0.34 for H_2O50-CDC. The sulfur was subsequently melt infiltrated at 155°C for 12 h under air.

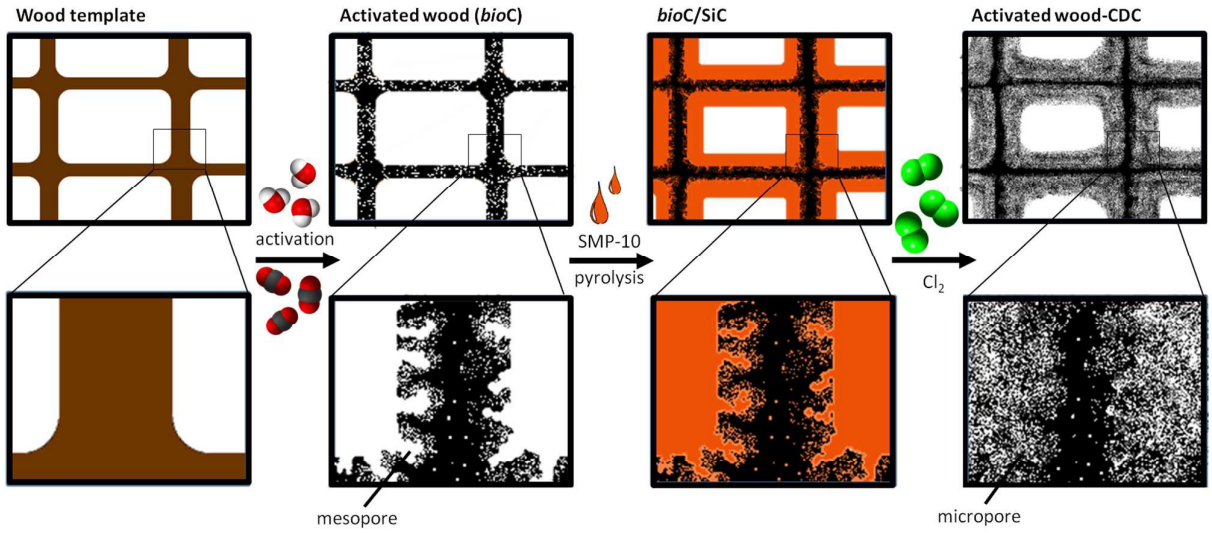

Figure 1 – Wood template is first activated with CO_2 or steam, resulting in activated wood (*bio*C) with typical wood microstructure and additional porosity, consisting of micro and mesopores. Followed by impregnation of macro-, meso-, and micropores with polycarbosilane (SMP-10) and pyrolysis, *bio*C/SiC composite is synthesized, which is treated with hot chlorine in the final synthesis step. Resulting activated wood-CDC material consists of macro-, meso-, and microporosity.

Electrode preparation. Cathodes were prepared from the C/S composites following a solvent-free roll-press procedure reported elsewhere[35]. The C/S composite was mixed with carbon nanotubes as conductive additive and PTFE binder in a weight ratio of 85 : 12 : 3. The typical active material loading of the punched circular electrodes with a diameter of 12 mm is 2 – 3 mg_{sulfur}/cm^2.

Electrochemical characterization. Lithium-sulfur half cells were prepared in an argon filled glove box (MBraun, < 0.1 ppm O_2 and < 0.1 ppm H_2O) by stacking the C/S composite cathode (working electrode), a porous polypropylene separator (Celgard 2500) and elemental lithium (MTI corp., counter and reference electrode) with 6.8 µl/mg_{sulfur} of electrolyte in CR2016 coin cells. The electrolyte consisted of 1 M LiTFSI and 0.25 M $LiNO_3$ in DME/DOL (Dimethoxy ethane/1,3-dioxolane) (1:1 by volume)). The rate capability tests at different discharge rates (discharge // charge rate of C/10 // C/10; C/5 // C/5; C/2 // C/5; 1 C // C/5; 2 C // C/5; 5 C // C/5; 1 C = 1672 mA/g_{sulfur}) were characterized at room temperature with a BASYTEC CTS cell test system. For increased polarization, the typical voltage range of 1.8 - 2.6 V vs. Li/Li^+ was readjusted to 1.6 - 2.6 V vs. Li/Li^+ at discharge rate of C/2 and to 1.4 - 2.6 V vs. Li/Li^+ at high discharge rates of 1 C and 2 C as well as to 1.2 - 2.6 V vs. Li/Li^+ at 5 C.

Results and discussion

Structure and porosity of activated wood-CDC. Hierarchically structured, activated wood-carbide-derived carbons were synthesized via activation of the bio-template with steam or carbon dioxide and a subsequent CDC approach, as shown in Figure 1. In contrast to already known synthetic templates used for the synthesis of hierarchical carbon structures such as DUT-86[36] or PolyHIPE-CDC[24], no time-consuming template synthesis and their removal is necessary. Furthermore wood offers a macroporous

Table 1 – Specific surface area, pore size, and pore volume of the activated *bio*Cs and activated wood-CDCs obtained with carbon dioxide- and steam-activation at different carbonization temperatures or with different steam saturation concentrations at 900 °C.

steam			Activated wood					Activated wood-CDC				
water temperature °C	steam saturation g/m^3	burn off[a] %	SSA m^2/g	micropore volume[b] cm^3/g	mesopore volume[b] cm^3/g	mesopore size nm	macropore size[c,d] µm	SSA m^2/g	micropore volume[b] cm^3/g	mesopore volume[b] cm^3/g	mesopore size nm	macropore size[c,d] µm
25	23.0	3.3	670	0.28	0.06	4.9	4.0	1090	0.43	0.12	3.2	2.2
50	82.8	4.8	815	0.26	0.12	4.9	4.0	1130	0.41	0.16	3.1	2.0
80	290.7	6.1	750	0.23	0.15	5.0	4.0	890	0.30	0.23	4.4	2.0
CO_2												
carbonization temperature °C		burn off[a] %	SSA m^2/g	micropore volume[b] cm^3/g	mesopore volume[b] cm^3/g	mesopore size nm	macropore size[c] µm	SSA m^2/g	micropore volume[b] cm^3/g	mesopore volume[b] cm^3/g	mesopore size nm	macropore size[c] µm
850		33.6	450	0.20	0.06	4.0	4.0	1330	0.40	0.33	3.3	2.2
900		38.6	580	0.21	0.09	4.4	4.0	1470	0.42	0.36	3.8	2.1
950		51.7	1080	0.41	0.27	6	4.5	1750	0.51	0.50	3.9	1.8

[a]burn off: weight loss due to activation process (weight loss due to carbonization of wood template of about 77 % is not included).
[b]Pore volumes calculated from nitrogen physisorption isotherms with QSDFT model.
[c] macropore size was determined by SEM images.
[d] macropore volumes were determined representatively with mercury porosimetry for H_2O50 and H_2O50-CDC with 1.3 and 1.2 cm^3/g, respectively.

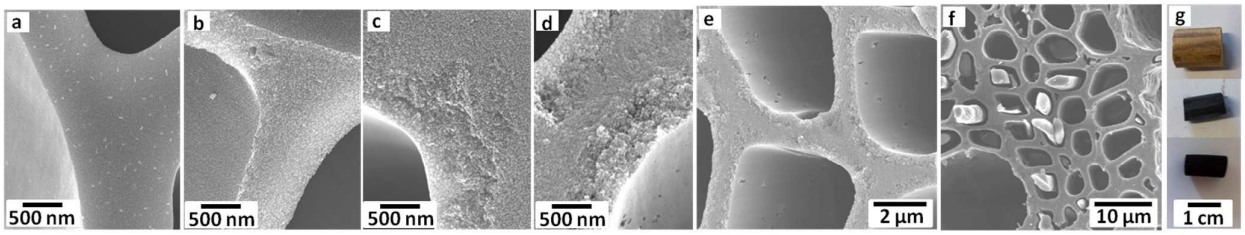

Figure 2 –SEM images of cell walls of pyrolyzed wood (a) and steam activated wood samples, activated with water of 25 °C (b), 50 °C (c), and 80 °C (d). SEM image of steam activated wood (H_2O50) prepared with 50°C warm water (e), and activated wood-CDC (H_2O50-CDC) (f), respectively. (g) Images of wood (top), activated wood (middle) and activated wood-CDC (bottom) monolith.

structure, which enables the possibility to produce sustainable, hierarchical porous carbon materials with 300 -30000-fold lower costs.

Biotemplate activation. Activated carbon monoliths were produced by treating wood monoliths at 900 °C with varying concentrations of water steam or at different temperatures with carbon dioxide. Weight losses (burn off), specific surface areas, pore volumes, and pore sizes of resulting activated wood monoliths are shown in Table 1.

The higher the carbonization temperature/the steam concentration, the higher the gasification amount, caused by the Boudouard equation ($CO_2 + C \leftrightarrow 2\ CO$, $\Delta_R H$= +172.5 kJ/mol) and/or the progressive partial oxidation of the carbon structure in both activation processes. SEM images in Figure 2 and 3 show that gasification of carbon partially damaged the cell walls, inducing many micro- and mesopores while preserving the unique cell structure of wood with longitudinal directed macropores and the monolithic structure. Pores size distributions (Figure 4 and 5) calculated with QSDFT method from low pressure nitrogen physisorption isotherms show the presence of a hierarchical micro-meso-type pore system. In combination with the SEM images, showing the preservation of macropores of about 4 µm (Figure 2 and 3), we could demonstrate the synthesis of a carbon material with trimodal pore system. Due to the pore formation by the activation process, *bio*C monoliths with SSAs up to 815 m^2/g in the case of steam activation and 1080 m^2/g in the case of carbon dioxide activation can be obtained. The SSAs of synthesized steam activated monoliths are in the same region as of activated wood powders discussed in the literature[20,21]. Hence, we could demonstrate that the utilization of monoliths in activation processes is also possible. As described before, steam activation under various conditions is performed in literature. Wu et al.[20] synthesized activated fir wood carbon under same conditions with slightly higher SSA but significant lower micropore amounts of only 51 % of the total micro-mesopore volume in contrast to 61-78 % for the steam activated wood samples presented here. Due to a reduced diffusion of the activating gas within the monoliths in comparison to powders, the activation process is less progressed explaining that the amount of micropores stays fairly above the values in the cited literature.

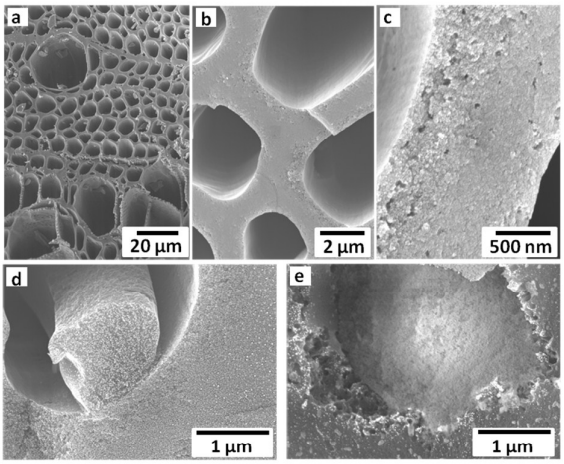

Figure 3 – (a-c) SEM images of carbon dioxide activated wood sample, prepared at 850 °C. SEM images of activated wood-CDC samples prepared with carbonization temperatures of 850 °C (d) and 950 °C (e), respectively.

The specific surface area of the resulting steam activated carbon materials increase when the water temperature is raised up to 50 °C. A further increase of the steam concentration leads to higher burn off, which results in progressive destruction of the wood walls and widening of the formed pores, resulting in a smaller SSA and higher mesopore volume. The determined nitrogen physisorption isotherms of type IV according to the IUPAC classification (Figure 4) show broadening hysteresis loops with higher water concentration, which imply the increasing presence of mesopores in the activated *bio*C structures. Regarding the pores size distributions, a significant increase of the small mesopores of 2 to 10 nm with increasing water content is observed, which explains the decreasing micropore amounts from 78 to 61 % ($V_{micro}/V_{micro+meso}$).

In this respect, the key challenge of this method is the optimization of the SSA, finding the right steam concentration/water temperature, where the gasification rate is high enough to introduce a huge number of micropores but not too high, preventing a pronounced destruction of the *bio*C. According to our results, 50 °C seems to be an appropriate temperature to meet the requirements.

Regarding the carbon dioxide activated wood samples, a slight increase of SSA with increasing carbonization temperature from 850 °C to 900 °C but a huge increase towards 1080 m^2/g at 950 °C is noticed. Compared to steam activated samples, nitrogen physisorption isotherms (Figure 5) with very small hysteresis loops are determined, showing the smaller mesopore amount. At this point, it has to be mentioned that the progressive carbonization at

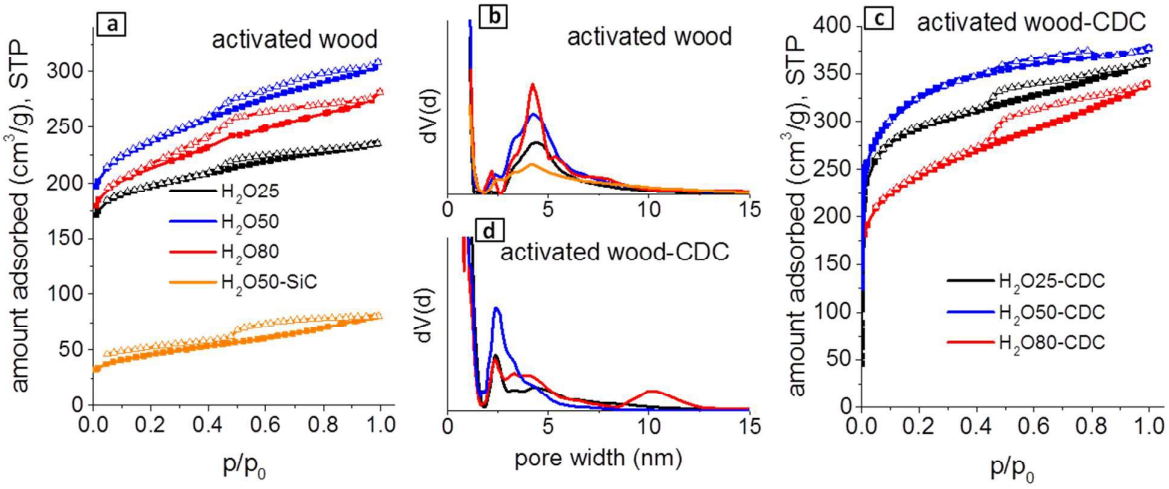

Figure 4 – (a) N_2 physisorption isotherms and (b) pore size distributions of steam activated wood samples, prepared with different steam concentrations and activated *bio*C/SiC prepared with steam from 50 °C warm water. (c) N_2 physisorption isotherms of activated wood-CDCs prepared with different steam concentrations and their corresponding pore size distributions (d). (STP: standard temperature and pressure).

950 °C causes a burn off of over 50 %, which results in a notable broadening of pore size distribution in addition to a decreasing micropore amount and severely destroyed cell walls, presented in Figure 3.

Activated wood-carbide-derived carbons. To receive a higher SSA, pore volumes (PV) and a small pore size distribution, the activation process was combined with the carbide-derived carbon approach[22]. Using an impregnation with pure polycarbosilane solution, the accessible macropores as well as meso- and micropores are filled with the silicon carbide precursor, as displayed in SEM images of the resulting CDC materials (Figure 2f and 3d,e), as well as nitrogen physisorption isotherms and pore size distributions of the *bio*C/SiC composites in comparison to the non-infiltrated activated wood samples (Figure 4a,b and 5a,c). The subsequent selective extraction of silicon atoms by chlorine treatment is associated with the formation of large amounts of micropores in the walls of the amorphous silicon carbide[37] (XRD pattern of amorphous bioC/SiC composite are shown in Figure S1). The carbon content of resulting activated wood-CDC materials estimated by EDX measurements is about 95 at.% (Table S1), with only residues of silicon and oxygen. TGA Measurements show complete conversion under air, witch confirm the high purity of the materials (Figure S2). As shown in Figure 2 and 3, macropores are still present, but partially filled with CDC material resulting in smaller average diameter of about 2 µm. Due to insertion of microporous CDC material in the activated wood structure the SSA and PV are improved up to 1130 m^2/g and 0.57 cm^3/g (Table 1) for steam treated samples. Moreover, the trend of an optimum SSA at 50 °C water temperature and the decreasing micropore amount with increasing activation temperature is maintained. Nitrogen physisorption isotherms and pore size distributions in Figure 4 show drastically higher amount of micropores, determined by the distinct uptake of nitrogen in low relative pressures ($p/p_0 < 0.1$), and less small mesopores of 4 – 8 nm in the CDC materials compared to the activated wood materials. This decrease in 4 - 8 nm mesopores and the simultaneous increase of smaller mesopores could be explained with the filling with polycarbosilane of the activated wood sample.

In the impregnation step the polycarbosilane solution penetrate into the template and fill micro-, meso-, and macropores. This infiltrated material ensures a narrowing or complete filling of these pores. The filling of the meso- and micropores by silicon carbide can be observed very well in the isotherms and associated pore size distributions, shown in Figure 4 and 5. Regarding the data of bioC/SiC and activated bioC samples (H_2O-50 and H_2O50-SiC), the bioC/SiC composits show a significant decrease of nanopores, especially of mesopores. This leads to a narrowing of the distribution. Additional micropores are introduced in the materials by conversion of SiC into CDC by chlorine treatment, yielding higher micropore volumes for resulting CDC materials. Hence, the incorporation of CDC material not only increases the SSA but also induces a pronounced narrowing of the pore size distribution, consisting of mainly micro and small mesopores. Remarkable in the pore size distributions is also a nearly similar distribution of small mesopores in all steam activated wood-CDC materials.

Regarding the carbon dioxide activated wood-CDCs, SEM images (Figure 3) show that also CO_2 activated *bio*C monoliths can be combined with CDC approach yielding in hierarchical carbon materials. With nitrogen physisorption measurements increasing SSA and PV at higher activation temperatures with more than 1700 m^2/g and 1 cm^3/g were determined. CO_2 as well as steam activated wood-CDCs are characterized by micropores, small mesopores up to 10 nm, and macropores (2 µm) of the wood template. Moreover, a narrowing of the pore size distributions for activated wood-CDCs in comparison to the activated *bio*Cs is noticed (Figure 5). This trend could be also observed by steam activated CDC samples. To the best of our knowledge, no carbon structure obtained from biotemplate with trimodal pore system and so high specific surface area was described in the literature so far.

By comparing activated wood-CDCs with CDCs from non-activated wood templates (also using 100% SMP-10, showing a surface area of 940 m^2/g)[25], it becomes evident that the activation methods

prior to the CDC approach leads to an appreciable enhancement of the specific surface area without a broadening of the pore size distribution. This can be decisively attributed to the better diffusion/transport of the polycarbosilane into the wood structure via the inserted pores within the cell walls. The received results show, that insertion of pores in the wood cell walls by activation process is a facile and efficient method for generating a high porosity and to increase the impregnability of the wood template. Higher silicon carbide and consequently, higher CDC contents can be achieved by this increased impregnability due to activation process, yielding high specific surface areas and pore volumes.

In conclusion, this combination of activation process and CDC approach by impregnation of biotemplates enables the possibility to obtain highly porous carbon materials with hierarchical trimodal pore system, high surface areas, and narrow pore size distribution for nanopores, interesting for versatile applications like catalysis, adsorption or electrochemical devices.

Electrochemical Performance. The highly distinctive interconnected trimodal pore system consisting of micro, meso, and macropores should be well suitable to build up a lithium sulfur battery with excellent rate capability. Thus, steam activated woods-CDC (H_2O50-CDC) with micro/ mesopore volume of 0.57 cm^3/g was evaluated in Li-S battery tests as a proof-of-principle. To investigate the influence of the prior activation process to the overall performance, a non-activated wood-CDC[25] was used as reference material. According to the low micro/mesopore volume, only 28 % of sulfur can be infiltrated inside the micro/mesopores of the reference material to maintain a sufficient void space for volume expansions during discharge process. The increased pore volume of the steam activated material (H_2O50-CDC) enables a sulfur content of 34 % without decreasing the accessibility of the well suitable pore system. The authors want to point out that for future Li-S technologies sulfur loadings of >70 % are required. Here, the authors focus in a first proof-of-principle on the promising properties in rate stability of activated wood-CDCs, knowing the need of further optimization of the system, with respect to sulfur loading. However, the low sulfur content of the pristine composites could be compensated by enlarging the sulfur loadings due to compression of the prepared dense electrodes. All materials infiltrated with sulfur are further labelled with _S at the end. For H_2O50-CDC_S as well as the reference, no sulfur peaks are detected in X-ray powder diffraction pattern after melt infiltration indicating that sulfur does exist in a completely amorphous state inside the pores of both carbon materials (Figure S4). Nitrogen physisorption measurements before and after sulfur infiltration (Figure S5) also evidence the favorable distribution of sulfur inside the smaller pores rather than the larger macropores due to the decreasing of micro/mesopore volume. TG measurements of the melt-infiltrated samles are in good agreement with the adjusted carbon to sulfur ratio (Figure S6). SEM images of the compressed electrodes show a very dense and smooth surface (Figure S7a,c) leading to a high sulfur loadings of 3 mg_{sulfur}/cm^2 for H_2O50-CDC_S and 2 mg_{sulfur}/cm^2 for reference material, respectively, eliminating the disadvantage of the low sulfur content[38,39]. To optimize the overall cell performance, electrodes with high sulfur loading as well as more importantly low

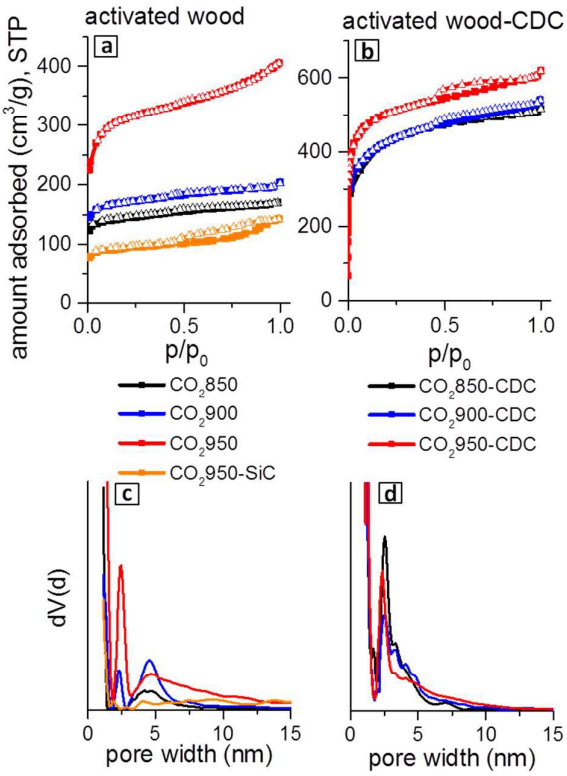

Figure 5 – (a) N_2 physisorption isotherms and (c) pore size distributions of CO_2 activated wood samples, prepared at different carbonization temperatures and activated *bio*C/SiC prepared with CO_2 at 950 °C. (b) N_2 physisorption isotherms of activated wood-CDCs synthezised at different carbonization temperatures and their corresponding pore size distributions (d).

electrode dead volume are absolutely necessary (dense electrodes) to achieve practical conditions. Despite densification of the electrodes, the macroporous network remains maintained (Figure S7b,d). In fact, these structural motifs, especially the pore geometry of wood can improve the high limitations of sulfur utilization at very high current densities due to the beneficial periodic ordered transport pores even using low excess of electrolyte. Considering that the trimodal pore system possesses unique synergetic properties, on the one hand, the micropores and small mesopores act as reaction chamber[40]. On the other hand, the macropores might improve the transport of the electrolyte, which is the most important kinetics limiting step at higher current densities. Consistently, the discharge capacities at varying current rates (Figure 6a) show only a slight loss of capacity even at rates as high as 2 C at a current density of 10.09 mA/cm^2. An initial discharge capacity of 865 mAh/g_{sulfur} (0.1 C, 0.5 mA/cm^2) and a stable capacity of over 580 mAh/g_{sulfur} (0.1 C to 1 C (5.05 mA/cm^2)) were achieved for H_2O50-CDC_S, whereas the reference composite shows lower capacities. However, the trend of the chart looks similar, which is in good agreement of our findings that the main difference of both wood-derived materials is only the microporosity. Therefore, the large 3D transport pores, evolutionary developed for optimized liquid transport over several 100 Mio years, are beneficial for low capacity losses at high C-Rates and, furthermore, the micro- and

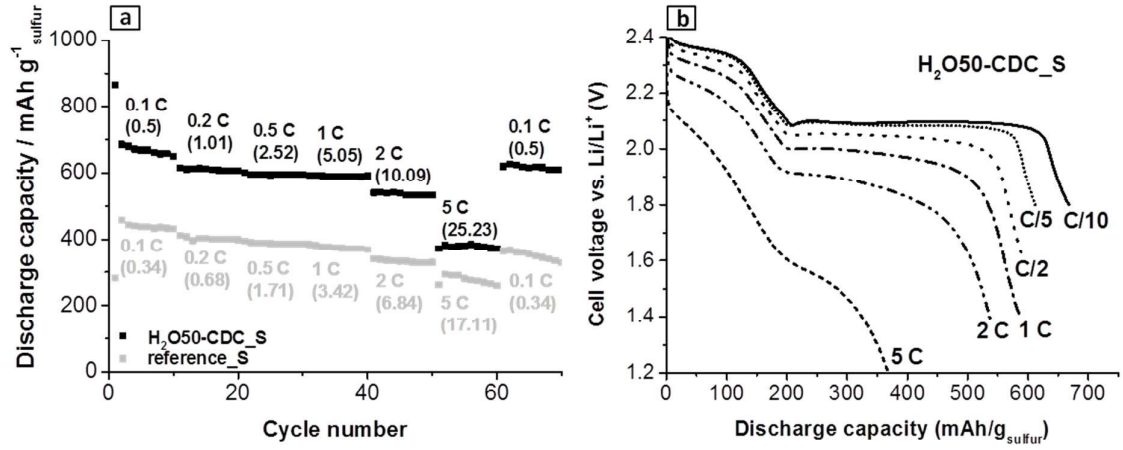

Figure 6 – (a) Rate capability test (C/10 – 5C). The values in brackets represent the corresponding current densities in mA/cm^2; (b) Typical discharge voltage profiles of H_2O50-CDC_S composite at different rates (taken from each 5 th cycle).

mesoporosity (small mesopores) mainly influence the sulfur utilizations, leading to a synergetic trimodal pore system[41,42] with good cycle stability (Figure 7). However, at a remarkable high current density of 25.23 mA/cm^2 (5 C) the discharge capacity starts to drop faster to 400 mAh/g_{sulfur} for H_2O50-CDC_S. The corresponding voltage profiles show low polarizations at moderate rates as can be seen from Figure 6b (for voltage profile of reference see Figure S8). The rate capability, with respect to the applicable current density of H_2O50-CDC_S, especially the low loss of capacity, is a outstanding result in compare to previous publications[32,36,43-47] with high rates.

Moreover, we only used an amount of electrolyte as low as 6.8 µl/mg_{sulfur}. The latter is essential in evaluating rate performance. A very high excess of electrolyte can feign a good rate performance by buffering the lithium polysulfides[47,48]. Further, a high excess of lithium in combination with a high excess of electrolyte can feign good cycle performance. To our knowledge, up to date no publication can achieve such a high sulfur utilization as well as discharge capacity stability at current densities exceeding 20 mA/cm^2 even using such a low amount of electrolyte. Although other sulfur host materials applied as high rate composite showed higher sulfur utilizations, the sulfur content was very low (0.4 – 0.8 mg_{sulfur}/cm^2) and faster capacity fading at increased C-Rates was observed[32,43-46]. Furthermore, a huge excess of electrolyte was used leading to a low system energy density as compared to the rather realistic conditions in our approach. In contrast, the second concept from literature with high sulfur loadings (>6 mg_{sulfur}/cm^2) and consequently high areal capacities shows only low C-Rates to avoid high current densities as well as low discharge capacities[46]. Nevertheless, even an ordered hierarchical porous carbon[36] DUT-86-2_S with micro- and meso-, but without macropores with similar sulfur loading shows strong capacity fading at high C-Rates (over 1 C), whereas the wood transport pores in wood-CDC materials can buffer further losses (Figure S9). Apart of that, further improvements of the wood activation process (improvement of microporosity) might increase the sulfur utilization to those levels that are achieved by benchmark materials (e.g. DUT-86-2_S) only at low rates.

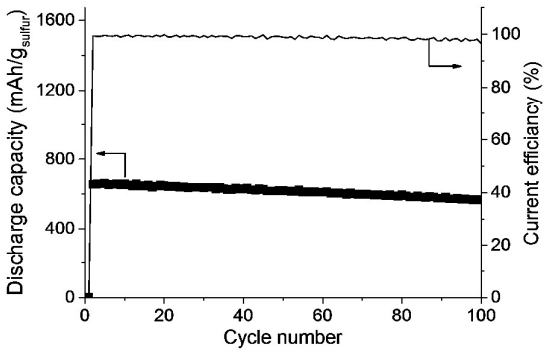

Figure 7 – Cycling stability of H_2O50-CDC.

Conclusions

We presented the synthesis of a trimodal hierarchical carbon by combining the activation with steam or carbon dioxide of wood templates with a subsequent CDC approach. Therefore, we mimic porous structures with cell anatomies that are optimized for mass transport during their long-term evolutional process as templates to setup the macropore structure of the material. We demonstrated that pre-treatment with steam or carbon dioxide inserts micro- and mesopores into the wood template and that subsequent impregnation with a silicon carbide precursor and halogen treatment yields significant higher SSA of the activated wood-CDC material in contrast to non-activated wood-CDC. This combination of different synthesis strategies with wood templates yields activated wood-CDC materials with specific surface areas up to 1130 m^2/g by steam activation and 1750 m^2/g by CO_2 activation. They offer narrow pores size distributions in the micro- and small mesopore range due to activation and CDC approach, while

maintaining the evolution-derived macropores of the wood template. This hierarchical biomorphic pore system ensures both, efficient mass transfer and high capacities, which makes activated wood-CDCs interesting as cathode material in Li-S batteries. The steam activated wood-CDC and a non-activated wood-CDC reveal excellent discharge capacity stability. Due to the higher surface area, pore volume and sulfur loading, higher capacities could be achieved with the activated sample. With this sample, a highly stable capacity of over 580 mAh/g_{sulfur} at current densities exceeding 20 mA/cm^2 (2 C) with high sulfur utilization and at very low amount of electrolyte of 6.8 µl/mg are possible. Making use of evolutionary developed pore systems and their functionalization could be also a promising strategy for other liquid phase applications where the subtle interplay of transport and storage requires complex hierarchical pore structures.

Acknowledgements

This work was funded by the DFG and European Social Fund ESF (Europäischer Sozialfonds) and the Free State of Saxony (Sächsische Aufbaubank - SAB), project No. 100111064. Lars Borchardt acknowledges the German Federal Ministry for Research and Education (BMBF) in support of the Mechanocarb project (award number 03SF0498). Stefan Kaskel would like to thank the DFG (KA 1698/18-1) for financial support.

References

1 L. Borchardt, F. Hasche, M. Lohe, M. Oschatz, F. Schmidt, E. Kockrick, C. Ziegler, T. Lescouet, A. Bachmatiuk, B. Buechner, D. Farrusseng, P. Strasser, S. Kaskel, *Carbon*, 2012, **50**, 1861-70.

2 G.-P. Hao, M. Oschatz, W. Nickel, M. Adam, S. Kaskel, *Curr. Org. Chem.* 2014, **18**, 1262-1279.

3 Y. Gogotsi, R. Dash, G. Yushin, T. Yildirim, G. Laudisio, J. Fischer, *J. Am. Chem. Soc*., 2005, **127**, 16006-7.

4 G. Yushin, E. Hoffmann, M. Barsoum, Y. Gogotsi, C. Howell, S. Sandeman, *Biomaterials*, 2006, **27(34)**, 5755-62.

5 J. Chmiola, G. Yushin, Y. Gogotsi, C. Portet, P. Simon, P. Tabema, *Science*, 2006, **313**, 1760-3.

6 L. Borchardt, M. Oschatz, S. Kaskel, *Materials horizon*, 2014, **1**, 157-68.

7 L. Borchardt, M. Oschatz, M. Lohe, V. Presser, Y. Gogotsi, S. Kaskel, *Carbon*, 2012, **50**, 3987-94.

8 V. Presser, M. Heon, Y. Gogotsi, *Adv. Funct. Mater*., 2011, **21**, 810-33.

9 M. Oschatz, E. Kockrick, M. Rose, L. Borchardt, N. Kein, I. Senkovska, T. Freudenberg, Y. Korenblit, G. Yushin, S. Kaskel; *Carbon*, 2012, **48 (14),** 3987-92.

10 H. Sieber, C. Rambo, J. Cao, E. Vogli, P. Greil, *Key Eng. Mater*., 2002, **206-213**, 2009-12.

11 P. Greil, T. Lifka, A. Kaindl, *J. Eur. Ceram. Soc*., 1998, **18**, 1961-73.

12 P. Greil, T. Lifka, A. Kaindl, *J. Eur. Ceram. Soc.,* 1998, **18**, 1975-83.

13 T. Ota, M. Takahashi, T. Hibi, M. Ozawa, S. Suzuki, Y. Hikidi, *J. Am. Ceram. Soc*., 1995, **78 (12)**, 3409-11.

14 H. Cheng, H. Endo, T. Okabe, K. Saito, G. Zheng, *J. Porous Mater.,* 1999, **6**, 233-7.

15 M. Patel, B. Padhi., *J. Mater. Sci. Lett*., 1993, **12**, 1234-5.

16 W. Qiao, Y. Korai, I. Mochida, Y. Hori, T. Maeda, *Carbon*, 2002, **40**, 351-8.

17 Z. Jin, G. Zhao, *BioResources*, 2014, **9(2),** 2237-47.

18 Z. Jin, G. Zhao, *BioResources*, 2014, **9(4),** 6831-40.

19 A.R. Sanchez, A.A. Elguezabal, L. de La Torre Saenz, *Carbon*, 2001, **39,** 1367-77.

20 F.-C. Wu, R.-L. Tseng, R.-S. Juang, *Sep. Puri. Techn*., 2005, **47**, 10-9.

21 N. Tancredi, T. Cordeo, J. Rodriguez-Mirasol, J.J. Rodriguez, *Sep. Sci. Techn*., 1997, **32(6)**, 1115-26.

22 Y. Gogotsi, A. Nikitin, H. Ye, W. Zhou, J. Fischer, B. Yi, H. Foley, M.W. Barsoum, Nature Mater., 2003, **2**, 591-4.

23 L. Borchardt, C. Hoffmann, M. Oschatz, L. Mammitzsch, U. Petasch, M. Herrmann, S. Kaskel, *Chem. Soc. Rev*., 2012, **41**, 5053-67.

24 M. Oschatz, L. Borchardt, M. Thommes, K.A. Cychosz, I. Senkovska, N. Klein, R. Frind, M. Leistner, V. Presser, Y. Gogotsi, S. Kaskel*, Angew. Chem. Int. Ed*., 2012, **51 (13)**, 7577-80.

25 M. Adam, M. Oschatz, W. Nickel, S. Kaskel, *Micro. Meso. Mater*., 2015, **210,** 26-31.

26 B. Scrosati, J. Hassoun, Y. K. Sun, *Energy Environ. Sci.,* 2011, **4**, 3287-95.

27 P. G. Bruce , S. A. Freunberger , L. J. Hardwick , J.-M. Tarascon , *Nat. Mater,*. 2012 , **11** , 19-29.

28 A. Manthiram, S. H. Chung, C. Zu, *Adv. Mater.,* 2015, **27**, 1980-2006.

29 X. Ji, K. T. Lee and L. F. Nazar, *Nature Mater*., 2009, **8**, 500–6.

30 X. Ji , L. F. Nazar , *J. Mater. Chem*., 2010 , **20** , 9821-26.

31 H. Yao, G. Zheng, P. C. Hsu, D. Kong, J. J. Cha, W. Li, Z. W. She, M. T. McDowell, K. Yan, Z. Liang, V. K. Narasimhan, Y. Cui, *Nat. Commun,*. 2013, **5**, 3943.

32 Z. Wei Seh, W. Li, J. J. Cha, G. Zheng, Y. Yang, M. T. McDowell, P.-C. Hsu , Y. Cui , *Nat. Commun.*, 2013 , **4** , 1331.

33 M. Rose, Y. Korenblit, E. Kockrick, L. Borchardt, M. Oschatz, S. Kaskel, G. Yushin, *SMALL*, 2011, **7(8),** 1108-17.

34 M. Oschatz, S. Thieme, L. Borchardt, M.R. Lohe, T. Biemelt, J. Brückner, H. Althues, S. Kaskel, *Chem. Commun*. , 2013, **49**, 5832-4.

35 S. Thieme, J. Brückner, I. Bauer, M. Oschatz, L. Borchardt, H. Althues, S. Kaskel, *J. Mater. Chem, A* 2013, **1**, 9225.

36 C. Hoffmann, S. Thieme, J. Brückner, M. Oschatz, T. Biemelt, G. Mondin, H. Althues, S. Kaskel, *ACS Nano,* 2014**, 8, 12**, 12130-40.

37 M. Oschatz, L. Borchardt, K. Pinkert, S. Thieme, M.R. Lohe, C. Hoffmann, M. Benusch, F.M. Wisser, C. Ziegler, L. Giebeler, M.H. Rümmeli, J. Eckert, A. Eychmüller, S. Kaskel, Adv. Energy Mater., 2014, **4**, 1300645-8.

38 L. X. Miao, W. K. Wang, A. B. Wang, K. G. Yuan, Y. S. Yang, J. *Mater. Chem. A,* 2013, **1**, 11659-64.

39 M. Wang, W. Wang, A. Wang, K. Yuan, L. Miao, X. Zhang, Y. Huang, Z. Yu, J. Qiu, *Chem. Commun*., 2013, **49**, 10263-5.

40 P. Strubel, S. Thieme, T. Biemelt, A. Helmer, M. Oschatz, J. Brückner, H. Althues, S. Kaskel, *Adv. Funct. Mater.,* 2015, **25**, 287-97.

41 X. Li, Y. Cao, W. Qi, L. V. Saraf, J. Xiao, Z. Nie, J. Mietek, J.-G. Zhang, B. Schwenzer, J. Liu, *J. Mater. Chem.,* 2011, **21**, 16603.

42 C. Liang, N. J. Dudney, J. Y. Howe, *Chem. Mater,.* 2009, **21**, 4724-30.

43 X. Yang, L. Zhang, F. Zhang, Y. Huang, Y. Chen, *ACS Nano* 2014, **8** (5), 5208-15.

44 G. He, X. Ji, L. Nazar, *Energy Environ.Sci*., 2011, **4**, 2878-83.

45 J. Schuster, G. He, B. Mandlmeier, T. Yim, K. T. Lee, T. Bein, L. F. Nazar, *Angew. Chem. Int. Ed,.* 2012, **51,** 3591-5.

46 L. Miao, W. Wang, K. Yuan, Y. Yang, A. Wang, *Chem. Commun.* 2014, **50**, 13231-4.

47 J. Brückner, S. Thieme, H. T. Grossmann, S. Dörfler, H. Althues, S. Kaskel, *Journal of Power Sources,* 2014, **268**, 82-7.

48 L. F. Nazar, M. Cuisinier, Q. Pang, *MRS Bulletin,* 2014, **39**, 436-42.